Neurotherapeutics 21 (2024) e00458

Contents lists available at ScienceDirect

Neurotherapeutics

journal homepage: www.sciencedirect.com/journal/neurotherapeutics

Original Article

Targeting the Hippo pathway in Schwann cells ameliorates peripheral nerve degeneration via a polypharmacological mechanism

Hyung-Joo Chung [a,1], Thy N.C. Nguyen [b,1], Ji Won Lee [c,1], Youngbuhm Huh [d], Seungbeom Ko [e], Heejin Lim [f], Hyewon Seo [g], Young-Geun Ha [h], Jeong Ho Chang [i], Jae-Sung Woo [j], Ji-Joon Song [k], So-Woon Kim [l], Jin San Lee [m], Jung-Soon Mo [n], Boyoun Park [o], Kyung-Won Min [c], Je-Hyun Yoon [e,p,*], Min-Sik Kim [b,*], Junyang Jung [d,*], Na Young Jeong [q,*]

[a] Department of Anesthesiology and Pain Medicine, College of Medicine, Kosin University, Busan 49267, South Korea
[b] Department of New Biology, Daegu Gyeongbuk Institute of Science and Technology (DGIST), Daegu 42988, South Korea
[c] Department of Biology, College of Natural Sciences, Gangneung-Wonju National University, Gangneung 25457, South Korea
[d] Department of Anatomy and Neurobiology, College of Medicine, Kyung Hee University, Seoul 02447, South Korea
[e] Department of Biochemistry and Molecular Biology, Medical University of South Carolina, Charleston, SC 29425, USA
[f] Center for Scientific Instrumentation, Korea Basic Science Institute (KBSI), Cheongju 28119, South Korea
[g] New Drug Development Center (NDDC), Daegu-Gyeongbuk Medical Innovation Foundation (K-MEDI hub), Daegu 41061, South Korea
[h] Department of Chemistry, College of Convergence Science, Kyonggi University, Suwon 16227, South Korea
[i] Department of Biology Education, Kyungpook National University, Daegu 41566, South Korea
[j] Department of Life Sciences, Korea University, Seongbuk-gu, Seoul 02841, South Korea
[k] Department of Biological Sciences, Korea Advanced Institute of Science and Technology (KAIST), Yuseong-gu, Daejeon 34141, South Korea
[l] Department of Pathology, College of Medicine, Kyung Hee University Hospital, Kyung Hee University, Seoul 02447, South Korea
[m] Department of Neurology, College of Medicine, Kyung Hee University Hospital, Kyung Hee University, Seoul 02447, South Korea
[n] Institute of Medical Science, School of Medicine, Ajou University, Suwon 16499, South Korea
[o] Department of Systems Biology, College of Life Science and Biotechnology, Yonsei University, Seoul 03722, South Korea
[p] Department of Oncology Science, College of Medicine, The University of Oklahoma, Oklahoma City, OK 73104, USA
[q] Department of Anatomy and Cell Biology, College of Medicine, Dong-A University, Busan 49201, South Korea

ARTICLE INFO

Keywords:
Schwann cells
Hippo/MST pathway
RNA-binding protein
let-7b
p38α/MAPK14

ABSTRACT

Peripheral neuropathies (PNs) are common diseases in elderly individuals characterized by Schwann cell (SC) dysfunction and irreversible Wallerian degeneration (WD). Although the molecular mechanisms of PN onset and progression have been widely studied, therapeutic opportunities remain limited. In this study, we investigated the pharmacological inhibition of Mammalian Ste20-like kinase 1/2 (MST1/2) by using its chemical inhibitor, XMU-MP-1 (XMU), against WD. XMU treatment suppressed the proliferation, dedifferentiation, and demyelination of SCs in models of WD *in vitro*, *in vivo*, and *ex vivo*. As a downstream mediator of canonical and noncanonical Hippo/MST1 pathway activation, the mature microRNA (miRNA) let-7b and its binding partners quaking homolog (QKI)/nucleolin (NCL) modulated miRNA-mediated silencing of genes involved in protein transport. Hence, direct phosphorylation of QKI and NCL by MST1 might be critical for WD onset and pathogenesis. Moreover, p38α/mitogen-activated protein kinase 14 (p38α) showed a strong affinity for XMU, and therefore, it may be an alternative XMU target for controlling WD in SCs. Taken together, our findings provide new insights into the Hippo/MST pathway function in PNs and suggest that XMU is a novel multitargeted therapeutic for elderly individuals with PNs.

Abbreviations: CC_{50}, half-maximal cytotoxic concentration; CCND1, cyclin D1; DARTS, drug affinity responsive target stability; DIV, days of *in vitro* culture; DPN, diabetic peripheral neuropathy; EC_{50}, half-maximal effective concentration; GI_{50}, half-maximal inhibition of cell proliferation; LAMP1, lysosomal-associated membrane protein 1; LATS1/2, large tumor suppressor 1/2; MAPK, mitogen-activated protein kinase; MBP, myelin basic protein; MST1/2, mammalian sterile 20-like kinase 1/2; PDB, protein data bank; p75 NTR, nerve growth factor receptor p75; SC, Schwan cell; WD, Wallerian degeneration; YAP, Yes-associated protein.

* Corresponding authors.
E-mail addresses: jehyun-yoon@ouhsc.edu (J.-H. Yoon), mkim@dgist.ac.kr (M.-S. Kim), jjung@khu.ac.kr (J. Jung), jnyjjy@dau.ac.kr (N.Y. Jeong).

[1] These authors equally contributed to this study.

https://doi.org/10.1016/j.neurot.2024.e00458
Received 15 June 2024; Received in revised form 3 September 2024; Accepted 22 September 2024

Introduction

Anterograde peripheral nerve degeneration, also known as Wallerian degeneration (WD), is a process essential for the initiating and completing peripheral nerve regeneration [1,2]. Irreversible WD leads to peripheral neuropathies (PNs) observed in age-associated pathologies of elderly individuals older than 65 years old [3,4]. Schwann cells (SCs), constituting a unique population of glial cells, regulate WD via their contribution to multifactorial biochemical events, and they induce various phenotypic alterations in peripheral nerves, such as demyelination and axonal degradation, and undergo dedifferentiation/proliferation [5]. Efficient control of relevant pathways composed of proteins and noncoding RNAs in SCs can prevent or slow WD progression. A few signaling pathways have been identified in WD [6], but no important single pathway has been thoroughly characterized in the literature to date.

The Hippo signaling pathway, or the Salvador-Warts-Hippo (SWH) pathway, is a cascade of protein kinases that regulate cell proliferation, growth, and apoptosis [7–11]. This pathway involves several biochemical events in SCs during peripheral nerve development and regeneration, including SC myelination, proliferation, and redifferentiation [12]. Mammalian sterile 20-like kinase 1/2 (MST1/2) and large tumor suppressor 1/2 (LATS1/2) are the main kinase components of the Hippo pathway; activated MST1/2 phosphorylates LATS1/2, which subsequently phosphorylate Yes-associated protein (YAP), the core effector of the Hippo pathway [9]. This phosphorylation relay results in the cytoplasmic retention of YAP, which leads to the inactivated expression of genes downstream of YAP [9]. Conversely, when the Hippo pathway is inactivated, YAP is translocated into the nucleus, where it promotes the transcription of downstream genes associated with cell proliferation, growth, and survival [8]. Thus, MST1/2, as the upstream components of the Hippo pathway, can trigger subsequent pathological signaling and might play an important role in SC dynamics during WD.

The selective MST1/2 inhibitor XMU-MP-1 (XMU, Supplementary Fig. 1a), a benzene sulfonamide, activates the downstream effector YAP, thereby promoting cell growth, proliferation, and regeneration [13]. Previous studies showed that XMU administration boosted intestinal epithelial cell repair and liver regeneration in mouse models of injury [13]. XMU treatment enhanced the survival of cardiomyocytes *in vitro* and preserved cardiac function in model mice *in* vivo [14]. Although a previous report showed that modulation of YAP levels did not affect WD after nerve injury, in contrast to its effect on SC development [15], the phosphorylation status of YAP might be a critical factor in WD. These prior studies indicated that canonical or noncanonical Hippo pathways are critically to WD and that the effects of multitargeted treatments on SCs may provide therapeutic benefits to prevent PNs more effectively.

In this study, we utilized in vivo, *ex vivo*, and *in vitro* models of WD to investigate the polypharmacological effects of XMU. Novel effectors downstream of the Hippo pathway, including RNA-binding proteins (RBPs)/mature microRNAs (miRNAs) [16] and p38α/MAPK14 (p38α), were discovered as novel targets of XMU. Our bio/chemoinformatics analyses revealed a particularly efficient search method for identifying drug targets and pharmacological mechanisms underlying WD prevention for treating PNs.

Methods

Animals

5 weeks-old male mice in C57BL/6 background used in this study were purchased from Orientbio™. All experimental animals were in the appropriate environment controlled with temperature (23 ± 1 °C) and humidity (50 %) on a 12-h light-dark cycle and provided with free access to feeds and water. All procedures in the animal experiment were tried to minimize the suffering of the mice and the number of animals according to the policies established by Kyung Hee University Committee on Animal Research. All animal experiment procedures, including sacrifices, were approved by Kyung Hee University Committee of Animal Research [KHSASP-21-463] and progressed according to the guidance prepared by Korean Academy of Medical Science.

Sciatic nerve explant culture and ex vivo transfection

Sciatic nerve explant was cultured as described previously [17]. Briefly, sciatic nerves surrounded by connective tissues were isolated from 5-weeks-old C57BL/6 male mice by using a fine iris scissor (Fine Science Tools) under a sterile surgical environment. The connective tissues were then removed in the phosphate-buffered saline (PBS) under a stereomicroscope. The isolated nerves were transferred into ice-cold PBS and then washed without any further damage. Afterward, each isolate was pieced by fine iris scissors into 3–4 mm size lengths. Then, the nerves were transferred into the cell culture medium, Dulbecco's modified Eagle's medium (DMEM; SH30243.01, Cytiva) containing 9 % (v/v) fetal bovine serum (FBS; SH30919.03, Cytiva), and 1 % (v/v) penicillin/streptomycin (30-022-CI, Corning). The sciatic nerve explants were then incubated for three days in a humidified chamber at 37 °C and 5 % CO_2, in the presence or absence of XMU, +/-let-7b RNAs with 5′-phosphoryl and 3′-hydroxyl groups (UGAGGUAGUAGGUUGUGUGGUU-Cy3, Integrated DNA Technologies), or +/-anti-let-7b DNAs (AACCACACAACCTACTACCTCA-Cy3, Integrated DNA Technologies) (Supplementary Table 1). Three days after incubation, the sciatic nerve explants were washed in PBS and fixed with 4 % paraformaldehyde (PFA).

Morphometric indices

To quantify WD, we utilized stripe index defined as the number of spirals or light/dark stripes (bands of Fontana) in a 2 mm-length nerve observed under an Axiophot upright microscope set up with differential interference contrast (DIC) filters (Carl Zeiss). The corresponding number assigned as a stripe index and roughly indicated the degree of WD. The amount of myelin with ovoid-like shapes was counted within 200 μm length in teased nerve fibers. The corresponding number was assigned as an ovoid index and used as a criterion for demyelination. The myelin index was selected as an indicator for evaluating demyelination by counting the number of double-consecutive lines stained with anti-MBP antibody (over 100 μm long) out of 100 nerve fibers/group.

Transgenic zebrafish caudal-fin nerve degeneration model

The care and maintenance of zebrafish were performed in accordance with the guidelines of the Kyung Hee University Committee on Animal Research with approval (Protocol number #KHSASP-21-302). Two strains of zebrafish were used in this study; AB/Tuebingen (TU) for wild-type and Tg(MBP:EGFP) transgenic line. The transgenic fish line was provided by the Zebrafish Center for Disease Modeling (ZCDM). All surgical procedures were performed according to a previous method [18]. Briefly, all zebrafish were anesthetized in 0.6 mM tricaine (ethyl 3-232 aminobenzoate methanesulfonate, E10521, Sigma-Aldrich) and then placed on a petri dish. A crush injury to the caudal fin was proceeded with fine forceps (11412-11, Fine Science Tools) by carefully pressing an area 0.5 mm from the proximal region of the caudal fin. Two groups of zebrafish were treated with or without 100 μM of XMU for 10 days. To visualize and analyze the nerve degeneration, the caudal fin nerves were observed under an Axiophot upright microscope installed with DIC filters.

Fluorescence in situ hybridization (FISH)

All pre-hybridization procedures proceeded in RNase-free experimental conditions at room temperature (RT). Frozen tissue without fixation was submitted as 5 μm sections on positively charged microscopy slides. Section slides were post-fixed with 4 % PFA for 20 min, washed

twice with 1 × PBS for 15 min each, and equilibrated in 5 × saline-sodium citrate [SSC, 20 × SSC (C-9003, Bioneer), diluted with 0.1 % active diethylpyrocarbonate (DEPC)] for 15 min. The section slides were incubated with 5 × SSC contained with 50 % formamide (F9037, Sigma Aldrich) and 40 μg/ml of salmon sperm DNA (16131, Intron) for 2 h at 58 °C prior to hybridization. Next, a hybridization mixture (5 × SSC, 50 % formamide, 40 μg/ml of salmon sperm DNA, and 2.5 μM of anti-let-7b-Cy3 as a let-7b probe) was added to the section slides and incubated at 58 °C for overnight. Post-hybridization washes were performed in 2 × SSC for 30 min at RT, followed by pre-warmed 2 × SSC at 65 °C for 1 h and 0.1 × SSC at 65 °C for 1 h. Afterward, for co-immunostaining, the section slides were incubated in primary antibody [anti-S100-β (S100); 1:1000, s2532, Sigma Aldrich] for 1 h at RT, subsequently washed with 1 × PBS for 10 min, three times. Then, the fluorescent secondary antibody (AlexaFluor-488 Donkey anti-mouse) was treated under light protection and incubated for 1 h at RT. After washing the section slides three times for 10 min each, section slides were counterstained with DAPI (10236276001, Roche) for 1 min at RT. At last, the section slides were resuspended in Gelmount (M01, Biomeda).

Drug affinity responsive target stability (DARTS)

SW10 cells were lysed with M-PER (78501, Thermo Fisher Scientific) for 10 min in RT supplemented with 20 × protease inhibitor cocktail (11 873 580 001, Roche) and phosphatase inhibitors [1 M Sodium Fluoride (201154, Sigma Aldrich), 100 mM β-glycerophosphate (G5422, Sigma Aldrich), 50 mM Sodium Pyrophosphate (S9515, Sigma Aldrich), and 200 mM Sodium Orthovanadate (S6508, Sigma Aldrich)]. After centrifugation in 18,000×*g* for 10 min at RT, the lysates were added with 10 × TNC [1 M Tris-HCl pH 8.0 (T1501, Duchefa), 5 M Sodium Chloride (S0520, Duchefa), 1 M Calcium Chloride (C1016, Sigma Aldrich)] buffer to make a final concentration of 1 × TNC buffer in the lysate. Then, the lysates were treated with XMU for a final concentration of 500 μM, incubated for 30 min at RT, and rotated on a rotator. Increasing concentrations of thermolysin (0–6 μg/ml, V4001, Promega) were administrated to lysates, and the resulting mixture was incubated for 10 min at RT. To stop proteolysis, 20 × protease inhibitor was added to each sample at a ratio of 1:20, mixed well, and placed on ice. GAPDH was selected as a loading control.

Fluorescence polarization assay

Fluorescence polarization (FP) experiment was performed as described previously [19]. Briefly, recombinant GST-NCL was incubated with 3 nM Cy3-labeled let-7b in assay buffer [20 mM HEPES (pH 7.4, 150 mM Sodium Chloride, 4 mM Magnesium Chloride, 10 mM DTT, 0.05 % NP-40, 0.5 % glycerol, and 1 U/μl RiboLock RNase inhibitor]) at RT. Polarization measurements were taken after 5 min of incubation between protein and RNA in a 96-well non-binding black plate (Corning) at RT using a Spectramax iD5 microplate reader (Molecular Device), with excitation and emission wavelengths 530 nm and 570 nm, respectively. The values of millipolarization units (mP) were plotted against NCL concentrations, and then curve fitting was carried out by nonlinear regression using a one-site binding model in GraphPad Prism.

Phosphorylation sites mapping by mass spectrometry

MST1 protein (14-624, Millipore) was incubated for 30 min at 37 °C with recombinant proteins (human QKI, human AGO2, human Dicer, human Drosha, and mouse NCL; 2 μg) and 0.25 mM ATP in 20 μL kinase reaction buffer (20 mM HEPES, 10 mM magnesium chloride, 12 mM glycerophosphate, 2 mM DTT, and 1 mM sodium orthovanadate), after which reaction mixtures were processed with Filter Assisted Sample Preparation (FASP). Briefly, protein samples were dissolved in 9 M urea and subjected to reduction with 5 mM tris(2-carboxyethyl) phosphine (Sigma Aldrich) at 60 °C for 45 min and to alkylation with 20 mM 2-Iodoacetamide (Sigma Aldrich) at 25 °C for 15 min. Samples were then cleaned with a 30-kDa Amicon Filter (UFC503096, Millipore) three times with the use of 9 M urea and twice with 30 mM Ammonium Bicarbonate. After proteolysis with trypsin (Promega) and chymotrypsin (Roche) at a 1:20 ratio for 12 h at 37 °C, the digested peptides were desalted and eluted with 0.1 % Trifluoroacetic acid in 60 % Acetonitrile. The extracted peptides were dried and subsequently resuspended in 7 μL 0.1 % Formic acid for LC-MS/MS performed with an LTQ-Orbitrap Velos instrument (Thermo Fisher Scientific) interfaced with a nanoLC-2D and nano-ACQUITY UltraPerformance LC system (Waters). Precursor and fragment ions were analyzed at resolutions of 30,000 and 7,500, respectively. Peptide sequences were identified from isotopically resolved masses in MS and MS/MS spectra extracted with and without deconvolution using Thermo Scientific Xtract software. Data were analyzed with Proteome Discoverer 1.3 software (Thermo Fisher Scientific) conFig. d with Mascot and Sequest search nodes and were searched against Refseq version 46 human entries with oxidation on Met, deamidation of Asn and Gln, and phosphorylation of Ser, Thr, or Tyr as variable modifications, and carbamidomethylation of Cys as a fixed modification. Tolerances for precursor and fragment masses were set to 15 ppm and 0.03 Da, respectively. A peptide validator node was used for peptide confirmation, and a 1 % false discovery rate cutoff was used to filter the data.

Biacore assay

The binding analysis of recombinant QKI to let-7b-biotin was performed as described [20] by using a Biacore 3000 instrument and BIA evaluation software. The 50–100 response units (RU) of let-7b-biotin were immobilized onto a streptavidin chip (SA chip, GE Healthcare) and diluted in a running buffer consisting of 10 mM HEPES, 150 mM Sodium Chloride, 1 mM DTT, and 0.025 % surfactant P20 at pH 7.4. Recombinant QKI was then injected at RT for 3 min onto the cell surface and allowed to dissociate under a running buffer for 8 min.

Molecular docking

The crystal structures of QKI and NCL (PDB codes, 4JVH and 1FJE, respectively) were used to calculate suitable binding conformations with binding affinity of hexameric let-7b microRNA. Molecular dockings were carried out by the program PyRx Virtual Screening Tool Autodock Vina Version 0.9.7, every RNA fragment 5 times per model, with the determination among 15 calculated values of the minimum docking energy. For running the software, PDB file was converted to PDBQT format via OpenBabelGUI program. The docking models were presented by PyMOL software (The PyMOL Molecular Graphics System, Version 2.0 Schrödinger, LLC.)

Results

XMU suppresses WD in vitro, ex vivo, and in vivo

As SCs dedifferentiate and proliferate during WD, we assessed the cell viability (half maximal inhibitory concentration, IC_{50}), cell death (half maximal effective concentration, EC_{50}), and growth inhibition (half maximal inhibitory growth concentration, GI_{50}) of XMU using a mouse SC line (the SW10 cell line) as a dedifferentiated SC model (Supplementary Fig. 1b–e). We also performed morphometric analysis to quantitate the degree of WD using an *ex vivo* sciatic nerve explant system and thus excluded macrophage effects [17]. Normal sciatic nerves (uninjured) show transverse stripes (bands of Fontana), which disappear during WD. On day 3 of *in vitro* culture (3DIV), injured nerves showed no stripes, in contrast to control nerves, and several stripes remained visible in XMU-treated nerves (Fig. 1a, c). On 3DIV, the degenerating nerve fibers showed myelin fragmentation and ovoid shapes, in contrast to the control fibers, while fewer XMU-treated nerve fibers were ovoid shaped, similar to control nerves (Fig. 1b, d). A Morphometric analysis using

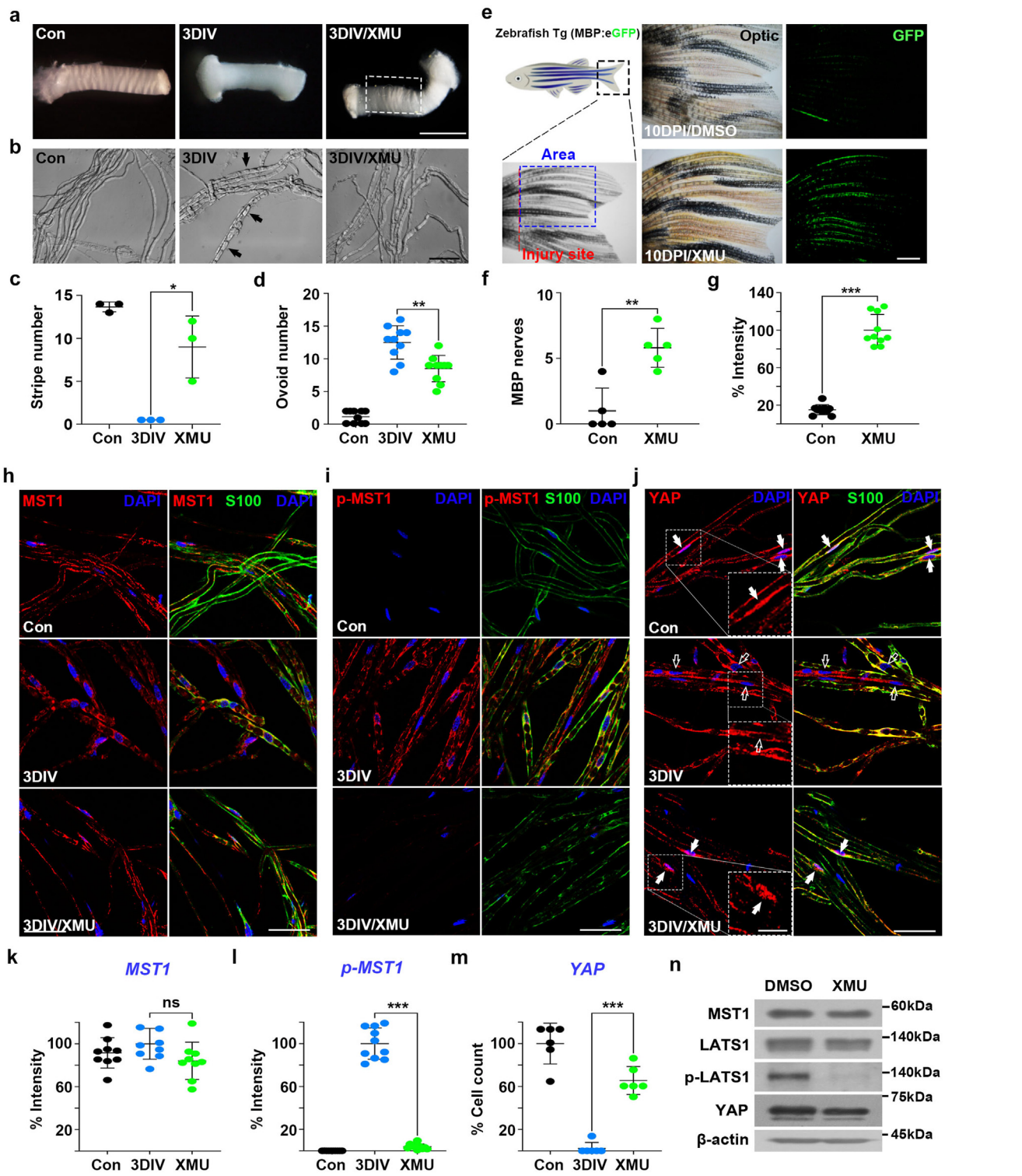

Fig. 1. XMU inhibits peripheral nerve degeneration. a, b Microscopy of the transverse stripes (*a*, Scale bar = 1 mm) and ovoid fragments (*b*, Scale bar = 50 μm) from the mouse sciatic nerve explants at three days *in vitro* (3DIV) in the presence or absence of XMU (100 μM). Control (Con) sample indicates the sciatic nerves right after explantation. Arrows (*b*) indicated the ovoids (myelin fragments). **c, d** Number of the stripes (*c*) and the ovoids (*d*) in **a** and **b**, respectively, were measured. **e** Transgenic adult zebrafish [Tg(MBP:EGFP) was used as *in vivo* WD model. Fluorescence images of zebrafish caudal fin were acquired at 10 days post-injury (DPI) with or without XMU treatment (10 μM) under a fluorescence stereoscope. Scale bar = 1 mm. **f, g** The number of intact GFP fluorescence (MBP nerves, *f*) and its intensity (MBP intensity, *g*) were measured at three areas (1×1 mm^2). **h-j** Expression patterns of MST1, phosphorylated MST1 at T183 residue (p-MST1), and YAP in *ex vivo* sciatic nerves at 3DIV in the presence or absence of XMU (100 μM). Scale bar = 50 μm. MST1 (*h*), p-MST1 (*i*), or YAP (*j*) were co-stained with either S100 (green, a marker of SCs) or 4′,6-Diamidine-2′-phenylindole (DAPI, blue). Dotted boxes indicated higher magnification images of the nucleus in Schwann cells (Scale bar = 20 μm). **k, l** Graphs showed the morphometric results of MST1 (% intensity, *k*) and p-MST (% intensity, *l*) in **h** and **i**, respectively. **m** Graphs showed the morphometric results of YAP (% cell counts) in (*j*). **n** Western blotting of hTERT02.3 cell lysates in the presence or absence of XMU (10 μM) showed the expression patterns of MST1, LATS1, phosphorylated LATS1 (p-LATS1), and YAP as components of canonical Hippo pathways in human SCs. *p < 0.05, **p < 0.01, ***p < 0.001, ns: not significant.

Tg(MBP:EGFP) zebrafish expressing EGFP in SCs [18] revealed that XMU prevented the disappearance of GFP signals 10 days post-injury (DPI) without inducing toxicity in adult fish (1–100 μM) (Fig. 1e–g).

Next, we measured the levels of MST1, which is a primary target of XMU, and that of its downstream proteins LATS1 and YAP in the canonical Hippo pathway. After XMU treatment of SCs, *ex vivo* immunostaining showed that signals emitted by phosphorylated MST1 (p-MST1) disappeared from the cytoplasm of SCs, while signals emitted from MST1 remained unaltered (Fig. 1h, i, k, l). YAP was translocated to the cytoplasm on 3DIV and XMU inhibited the translocation of YAP, suggesting its function as a transcription regulator of SC myelination and differentiation [21] (Fig. 1j, m). Western blot analysis with the hTERT02.3 human SC line also exhibited decreased levels of phosphorylated LATS1 after XMU treatment without changing the LAST1 levels (Fig. 1n). These results demonstrate that XMU inhibits canonical MST1-LATS1-YAP cascade signaling during WD.

XMU regulates the acquisition of degenerative phenotypes by SCs during WD

Peripheral nerves consist of peripheral nerve axons and SCs, the latter being core regulators of WD. To assess the inhibitory effect of XMU on demyelination mediated by SCs, we performed *ex vivo* immunostaining with myelin basic protein (MBP)-specific antibodies (a marker of the myelin sheath). Our results revealed that the fibers on 3DIV presented as several ovoid-like shapes, and the stain lines were disconnected, while the XMU-treated fibers resembled doubled continuous lines in the fibers comprising control cells (Fig. 2a, d). As a negative regulator of myelination and inducer of dedifferentiation genes [22], c-JUN is phosphorylated, activated, and then transported to the nucleus of SCs during WD [23], and this translocation was abolished in XMU-treated fibers, similar to the in fibers comprising control cells (Fig. 2b, e). As a marker of cell proliferation, KI67-positive signals were increased and overlapped with DAPI signals, but we observed no detectable KI67-positive signals in the nucleus of XMU-treated fibers, similar to fibers comprising control cells (Fig. 2c, f). As markers for the dedifferentiation of SCs, lysosomal-associated membrane protein (LAMP1) and p75 neurotrophin receptor (p75) levels in the fibers on 3DIV but not in XMU-treated fibers was increased, similar to levels in the control fibers (Fig. 2g and h). Immunoblots showed that XMU treatment reduced the levels of cyclin D1 (CCND1), LAMP1, and p75 on 3DIV (Fig. 2i). These results demonstrated that the canonical Hippo pathway is regulated by XMU in SCs *ex vivo*, as XMU effectively controls gene expression during WD.

Next, to determine whether the Hippo/MST1 pathway component expression is regulated at the transcriptional level by XMU in dedifferentiated SCs, we first selected two transcriptome datasets generated with C4-2 and 786-O cells treated with XMU (the GSE186177 and GSE197468 datasets, respectively; Supplementary Fig. 2a). Our analysis of differentially expressed genes (DEGs) revealed that the expression of Hippo signaling genes relevant to SC dynamics (development, degeneration, or regeneration), including *BMP8B*, *CCND1*, *BMPR2*, *SMAD4/7, BIRC2/3, DVL1/WNT5A/FZD8, WWC1,* and *FRMD6,* was altered [24–32]. We validated the levels of these DEGs by using mouse SW10 cells in a subsequent assay (Supplementary Fig. 2b).

Since transcription factors play critical roles in the myelination and dedifferentiation of SCs [33], we profiled 48 transcription factors selected from injured mouse sciatic nerves [34]. Among 12 transcription factors (*ATF3, E2F1, FOS, JUN, KLF10, NFYA, PLAGL1, RUNX1, SOX4, TGIF1, MYC*, and *THYN1*) that overlapped among three datasets (Supplementary Fig. 2c), *JUN* was the major negative regulator of myelin differentiation and drove SC dedifferentiation during WD (Fig. 2b, e) [22, 33], forming homodimers or heterodimers with *FOS* or *ATF3* to induce transcription activation [35]. Changes in transcription factor mRNAs were validated by qRT–PCR using SW10 cells (Supplementary Fig. 2d). Gene Ontology (GO) analysis of the shared 270 transcription factors (Supplementary Fig. 2e) exhibited enrichment of gene sets involved in cell differentiation/cell cycle/cell proliferation/anatomical structure morphogenesis (Supplementary Fig. 2e), and Kyoto Encyclopedia of Genes and Genomes (KEGG) analysis revealed 20 pathways most closely related to lipid–atherosclerosis/cell cycle/mitogen-activated protein kinase (MAPK) signaling (Supplementary Fig. 2f), common characteristics of degenerating SCs (Fig. 2).

XMU regulates positive protein transport in dedifferentiated Schwann cells

To assess the expression patterns of proteins regulated by XMU in dedifferentiated SCs, we performed global proteomics using the SW10 Schwann cell line. First, we conducted a hierarchical GO analysis, and six groups were classified on the basis of the upregulated proteins identified: transport (group 1), lipid metabolic process (group 2), responsive to stimulus (group 3), regulation of biological process (group 4), and cellular component organization (group 5) (Fig. 3a). Among GO terms in group 1, protein transport was the most enriched term and was related to the highest gene count, meaning that the proteins expression was upregulated under differentiated/myelinated conditions are associated with nuclear translocation of proteins in SCs (Fig. 3b). These findings were validated by qRT–PCR analysis using RNA samples purified *ex vivo* from sciatic nerves (Fig. 3c). The levels of mRNAs encoding proteins involved in protein transport were reduced during *ex vivo* WD, and their levels were partially recovered by XMU treatment (Fig. 3c). These results demonstrated that XMU alters the transcription profiles of dedifferentiated SCs via the Hippo/MST1 pathway.

Next, we screened proteins related to neuropathy (NP), a common irreversible form of WD. Disease-related genes (NP, n = 484) were obtained from DisGeNET [36]; 181 proteins identified are presented in a Venn diagram (Fig. 3d). Our GO analyses using the 181 proteins showed that the protein transport term was highly enriched (Fig. 3e). Among the 181 proteins, we found 12 transcription factors that mediated acquisition of SC degenerative phenotypes via nucleocytoplasmic transport (Fig. 3f). Among these 12 discovered proteins, ATF3/c-JUN (Supplementary Fig. 2c) and YY1 had been previously established as negative and positive regulators under differentiation/myelination conditions, respectively [35,37]. We verified that p-c-JUN, the active form of c-JUN, was expressed in SW10 cells by using western blotting and discovered that XMU exerted an inhibitory effect on p-c-JUN in dedifferentiated SCs (Fig. 3f). To elucidate the XMU-dependent protein transport of transcription factors, a network analysis was also performed in STRING-DB with the 12 transcription factors and 77 genes relevant to protein transport (Fig. 3b). We found that JUN was likely a highly active hub within the network (Fig. 3g), indicating a strong association between c-JUN and protein transport, similar to our *ex vivo* tissue data (Fig. 2b, e). Taken together, these data suggested that inhibition of the Hippo pathway can alter protein transport in SCs.

XMU modulates posttranscriptional regulation of protein transport genes via microRNAs during WD

Next, we tried to find trans-acting proteins and RNAs that mediate steady-state level changes in the levels of WD-relevant mRNAs. Since the Hippo/MST1 pathway modulates gene expression at the post-transcriptional level [9], we aimed to show that the MST1 pathway contributes to protein transport in SCs (Fig. 3a) by influencing mRNA decay, localization, and translation. First, we hypothesized that the protein transport genes listed in Supplementary Table 2 are targeted by regulatory noncoding RNAs such as miRNAs in a Hippo/MST1-dependent manner. Therefore, we profiled miRNAs predicted to target these mRNAs and identified a group of miRNAs, namely, mouse let-7 family miRNAs, miR-124-3p, miR-142-3p, miR-30-5p, and miR-384-5p (Supplementary Table 3). A small RNA sequencing (RNA-seq) analysis revealed that the levels of these miRNAs were changed in SW10 cells after XMU treatment (Supplementary Fig. 3a and Supplementary Table 4). qRT–PCR validated these findings (Supplementary

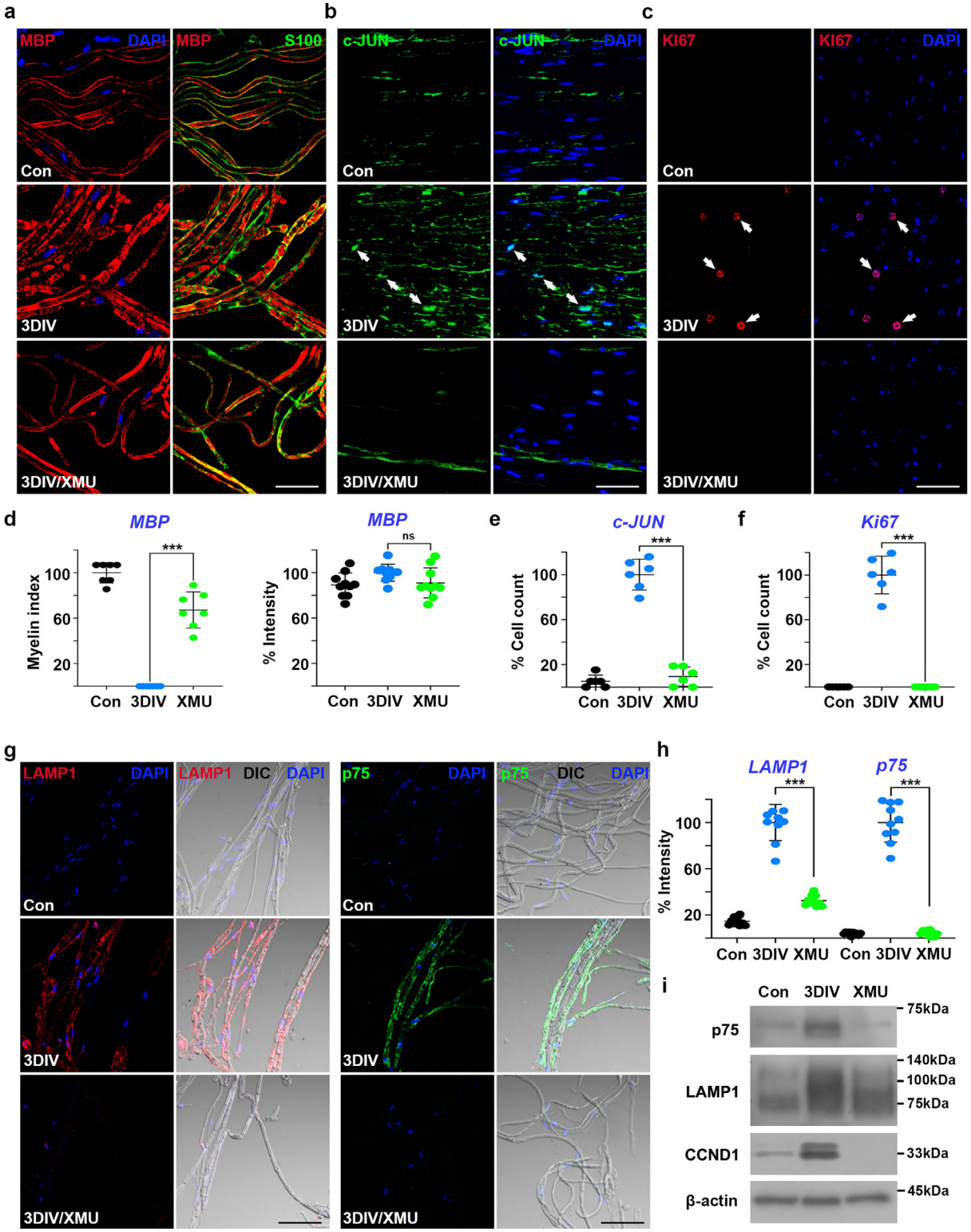

Fig. 2. XMU ameliorates degenerative characteristics in SCs. a-c Expression patterns of markers of demyelination (MBP, red; *a*), negative regulator for myelination (c-JUN, green; *b*), and proliferation (Ki-67, red; *c*) in *ex vivo* sciatic nerve fibers at 3DIV in the presence or absence of XMU (100 μM). S100 (green) and DAPI (blue) were co-stained with each marker. Control (Con) was non-injured sciatic nerves. The teasing samples, longitudinal sections, and cross-sections of the sciatic nerve were used for staining MBP, c-JUN, and KI-67, respectively. Scale bar = 50 μm. **d** Myelin index was the number of consecutive double-lines of MBP in each sample. Percent intensity of MBP signals was quantified by counting the relative number of pixels showing each intensity. **e, f** Percentage of cell counts indicated the number of c-JUN/DAPI (*e*) or KI-67/DAPI (*f*) double-positive nuclei in each sample. **g** Immunofluorescence in sciatic nerve fibers stained with lysosomal-associated membrane protein 1 (LAMP1, red) or p75 neurotrophin receptor (p75, green) as markers of SC dedifferentiation and DAPI (blue). Scale bar = 50 μm. **h** The graph showed the intensity of LAMP1 and p75 staining in sciatic nerve fibers cultured with 100 μM of XMU for 3DIV. **i** Western blot analysis of p75, LAMP1, and cyclin D1 (CCND1, a cell proliferation marker) levels in *ex vivo* sciatic nerve lysates. β-actin is a loading control. ***$p < 0.001$, ns: not significant.

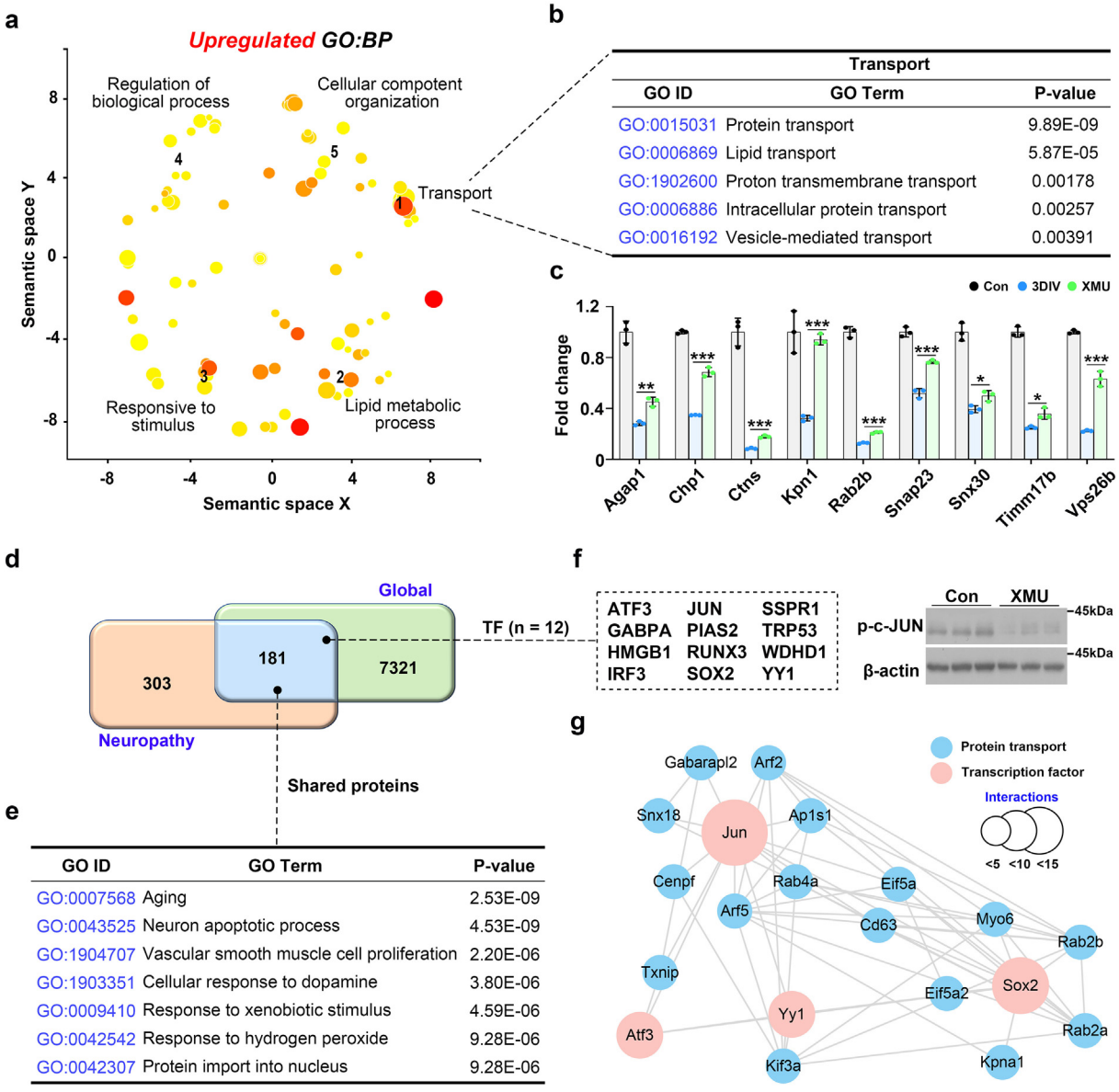

Fig. 3. XMU alters protein expression in dedifferentiated SCs. a. Gene Ontology (GO) analysis was performed on upregulated proteins in XMU-treated SW10 cells compared with control cells using a threefold (log_2 value) upregulated cutoff. A GO scatter plot was shown using Reduce and Visualize Gene Ontology (REVIGO). GO terms are represented by the bubbles, and the colors are meant as the *P* values. **b.** Representative GO terms of group 1 were shown, and they were selected among the phenotypic GO terms in Schwann cells. **c.** XMU-dependent genes involved in protein transport are validated via qRT-PCR. The nine genes were downregulated at 3DIV. Mouse sciatic nerve explants were used for the validation. *p < 0.05, **p < 0.01, and ***p < 0.001. **d.** Venn diagram showing the comparison of 484 genes associated with neuropathy (NP), and proteins from global proteomics. Proteins for NP (UMLS CUI#C0442874) were collected from the DisGeNET (v7.0) database. Transcription factor, TF. **e.** GO terms analysis by using the 181 proteins. **f.** 12 shared transcription factors are represented in the black square boxes. The expression of p-c-JUN was validated by Western blot analysis in SW10 cells. **g.** Functional protein association network of genes shown in key transcription factors and genes involving in protein transport. The size of the circle represents the STRING interaction score.

Fig. 3b and c) as indicated by the levels of three miRNAs, let-7b, let-7c, and let-7i, in the let-7 family, which were the most prevalent among the top-ranked downregulated miRNAs targeting the aforementioned genes (Supplementary Fig. 3a). GO and KEGG analyses revealed enrichment with miRNAs associated with the regulation of protein transport (GO:0051049) and the Hippo signaling pathway (Supplementary Fig. 3d and e).

Among the miRNAs involved in the posttranscriptional regulation of protein transport gene expression (Supplementary Table 3), we selected let-7b, a let-7 family miRNA, for further evaluation. Through *ex vivo* fluorescence *in situ* hybridization (FISH) analysis using anti-sense let-7b-Cy3 DNA, we observed that the number of positive signals was increased in the SC cytoplasm on 3DIV but not in XMU-treated fibers, similar to the respective controls (Fig. 4a). In an *ex vivo* phenotype analysis (Supplementary Fig. 4a), transfection of let7b RNA (Fig. 4b) resulted in stripe disappearance (Fig. 4c), ovoid shaped and fragmented myelin (Fig. 4d), and a decline in the expression of target mRNAs, such as *Snap23* and *Tram2* (4e, f), even in the presence of XMU in SCs (Supplementary Fig. 4b–d, Box B). Anti-sense let-7b DNA was introduced to *ex vivo* sciatic nerve culture to increase the number of phenocopies by 3DIV via XMU action (Fig. 4-f and Supplementary Fig. 4e and f). Besides the morphological similarity, biochemical phenotype markers, such as MBP, Ki67, c-JUN, p75 and LAMP1 in Fig. 2, were effectively inhibited after *ex vivo* anti- sense let-7b treatment (data not shown). However, transfection of

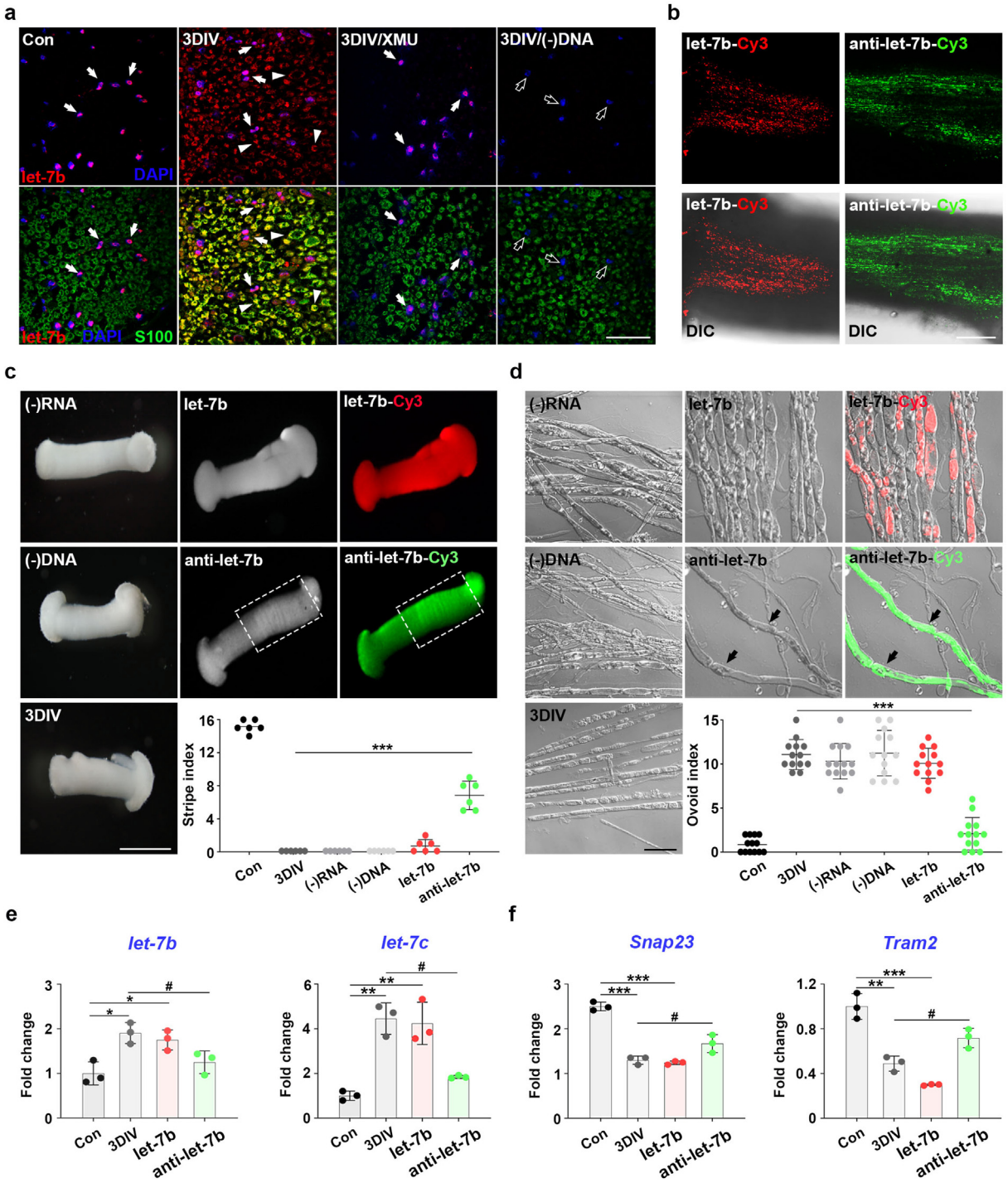

Fig. 4. Mature miRNA let-7b mediates MST1-dependent WD. a *Ex vivo* FISH showing let-7b enrichment and subcellular location in sciatic nerve fibers using anti-let-7b-Cy3 DNA (let-7b probe) in the presence or absence of XMU. Scale bar = 50 μm. miRNA-FISH (red) was co-stained with either S100 (green) or DAPI (blue). DNA [(-)DNA, TTGACAGGCAACCCCAACCA] template was used as a negative control. Arrows and arrowheads indicated anti-let-7b/DAPI and anti-let-7b/S100 double-positive signals, respectively. Blank arrows also indicated the nuclei with no signals of anti-let-7b-Cy3. **b** Sciatic nerve explants transfected with let-7b (1 μM) or anti-let-7b (1 μM) labeled with Cy3 were observed via confocal microscope at 3DIV. Scale bar = 200 μm. Transfected nerve fibers were shown as red (let-7b) and green (anti-let-7b). **c** Transverse stripes in let-7b-Cy3 (RNA)- or anti-let-7b-Cy3 (DNA)-transfected *ex vivo* samples at 3DIV. RNA [(-)RNA, GCGCGCUUUGUAGGAUUCG] or (-)DNA (*a*) templates were used as negative controls. Graphs displayed the stripe number of each group. Dotted boxes indicated transverse stripes. Scale bar = 1 mm. **d** Differential interference contrast (DIC) or fluorescence images of ovoid fragments in let-7b-Cy3 (RNA)- or anti-let-7b-Cy3 (DNA)-transfected *ex vivo* samples at 3DIV. Black arrows indicated Cy3-labeled nucleotides-transfected nerve fibers protected from WD. The graph showed the ovoid numbers of each group. Scale bar = 50 μm. **e** qRT-PCR validation of let-7b and let-7c in *ex vivo* sciatic explants. **f** *Snap23* and *Tram2*, genes involved in protein transport, were validated via qRT-PCR in *ex vivo* sciatic explants. * ^{or} $^{\#}p < 0.05$, $^{**}p < 0.01$, and $^{***}p < 0.001$, ns: not significant.

negative DNA or RNA did not affect the acquisition of degenerative phenotypes (Fig. 4c and d). These results demonstrated that let-7b is a miRNAs in SCs that mediates Hippo/MST1-dependent protein transport during WD.

MST1-mediated and miRNA-induced gene silencing by direct phosphorylation of multiple RNA-binding proteins

We wanted to determine how the Hippo/MST1 pathway modulates mature miRNA abundance during WD. The possibilities included regulation of primary miRNA production, precursor miRNA processing, and mature miRNA degradation [38,39]. An *in vitro* phosphorylation assay revealed direct phosphorylation of Drosha, Argonaute 2 (AGO2), and Dicer, which are miRNA processing and maturation enzymes [40–42]. The Drosha and miRNA complex structure was ascertained on the basis of the cryogenic electron microscopy (cryo-EM)-resolved structure of human Drosha and DGCR8 dimer in complex with pri-miR-16-2 at 3.7 Å resolution (Supplementary Fig. 5a) [41,43]. Human MST1 mediates the phosphorylation of AGO2 at T944 in a mobile basic (MB) helix and T1286 in a dsRNA-binding domain (dsRBD), which is critical for RNA binding (Supplementary Fig. 5b and c). AGO2 is also phosphorylated at S387 and T830 in a disordered loop [44], which is distant from the miRNA-binding pocket (Supplementary Fig. 5d and e). The human Dicer structure as observed via cryo-EM at a 4.7 Å resolution revealed that the S1115 and S1116 phosphosites are close enough to the binding site of precursor let-7 miRNA to influence its binding (Supplementary Fig. 6). These results indicated that direct phosphorylation of miRNA processing enzymes by MST1 affects the abundance of mature miRNA.

Among various RBPs relevant to mature miRNA function, RBPs directly binding mature miRNA let-7b and phosphorylated by MST1 in SCs during WD were newly identified. RBP Quaking (QKI) is the most relevant protein in connection with demyelination due to the clear phenotype acquisition it induces: mice lacking the *QKI* gene show accelerated demyelination and neuronal degeneration in the brain [45]. The level of QKI5, but not QKI6 or QKI7, declined in response to XMU treatment in hTERT02.3 cells (Supplementary Fig. 7a and b), whereas QKI5 was overexpressed/accumulated in the nuclei of SCs on 3DIV *ex vivo* and relocalized to the cytosol after XMU treatment (Fig. 5a, c). Another protein with high binding affinity for let-7b, nucleolin (NCL) [46], was also overexpressed during *ex vivo* WD and accumulated in the nucleus of SCs. Notably, these effects were suppressed by XMU treatment, after which NCL returned to nuclei, similar to its localization in control cells (Fig. 5b, d).

Direct binding of recombinant QKI and mature miRNA let-7b was modeled, and the accuracy of the model was confirmed by Bioacore assay, confirming its high affinity for let-7b (K_d = 11 nM) (Fig. 5e). The dissociation constant (K_d) = 3.745 nM indicated that recombinant GST-NCL [19,47] tightly bound let-7b (Fig. 5f). Both QKI and NCL had been previously shown to bind with other miRNAs and regulate their expression [48–51]. After QKI or NCL was overexpressed in SW10 cells, 9 mRNAs encoding proteins relevant to protein transport were downregulated (Fig. 5g and h), as we observed in *ex vivo* sciatic nerves after XMU treatment (Fig. 3c). Depletion of QKI or NCL resulted in opposite changes in the levels of target mRNAs (Fig. 5i and j). These results are similar to those of previous studies showing that QKI is a miRNA-dependent regulator of YAP transport [52,53] and that NCL regulates the nuclear transport of proteins [54].

Next, we evaluated whether recombinant QKI is directly phosphorylated by MST1. After incubation of those proteins in the presence of ATP and MST1, our mass spectrometry analysis revealed that MST1 phosphorylated QKI S188, which is close to the 5' end of the predicted let-7b-binding site (Supplementary Fig. 7c). NCL is also directly phosphorylated by MST1 at a T584 residue in mice (T587 in humans), although no clear protein structures have yet been reported (Supplementary Fig. 7d). These results indicated that QKI and NCL are novel substrates of MST1 that modulate QKI- and NCL-mediated posttranscriptional gene expression in SCs.

p38α is a novel target of XMU in Schwann cells

As a multifactorial cellular event, WD is simultaneously mediated via multiple proteins, complexes, and pathways, such as the WNT, MAPK, phosphatidylinositol 3-kinase (PI3K), and Hippo pathways [7,11]. To identify novel targets of XMU with the potential for effective pharmacological modulation of WD in SCs, we first profiled key signaling molecules involved in protein phosphorylation events and conducted quantitative phosphoproteomics by using SW10 cells treated with XMU (Supplementary Table 5). Among the phosphosites we profiled, the enriched GO terms and KEGG pathways included cellular functions such as protein phosphorylation, nucleocytoplasmic transport, MAPK signaling pathway, miRNAs, and longevity regulating pathway (Supplementary Fig. 8a and b). We also screened genes related to two diseases, namely, noninsulin-dependent diabetes mellitus (DM) and PN, to analyze proteins involved in diabetic peripheral neuropathies. The 3 proteins common to these diseases (p38α, GSK3B, and ATM) are presented in a Venn diagram and block box (Supplementary Fig. 8c).

We also identified key kinases [47] as target proteins of XMU. These kinases regulated protein phosphorylation in dedifferentiated SCs. Specifically, we performed kinase–substrate enrichment assays, and found 22 kinases that were downregulated in SCs after XMU treatment (Fig. 6a and Supplementary Table 6). Furthermore, to predict the strengths of the interactions between XMU and each of the 12 most downregulated kinases, we performed a binding affinity analysis and observed that p38α, mitogen-activated protein kinase kinase 1 (MEK1), AKT1, and ribosomal S6 Kinase 2 (RSK2) showed lower binding free energies than the other candidates (Fig. 6b and Supplementary Fig. 9). In particular, p38α showed both the lowest binding free energy with XMU and a tight association with the two diseases (Supplementary Fig. 8c) or SC functional dynamics [23,55,56]. In *ex vivo* immunostaining and western blotting, p38α was highly expressed in both the nuclei and cytoplasm of SCs on 3DIV, while XMU treatment inhibited p38α expression in nerve fibers, which was similar to that in the control fibers (Fig. 6c, e, f). The level of phosphorylated p38α (p-p38) on 3DIV was also measured in the nuclei of SCs during WD, and XMU was shown to inhibit its expression effectively (Fig. 6d, f).

A drug affinity responsive target stability (DARTS) assay [57] with SW10 cell lysates showed that the stability of p38α was increased by XMU treatment, suggesting a close interaction of XMU with the p38α protein (Fig. 6g). These results indicated that p38α is a novel target of XMU in SCs during WD.

Discussion

In the canonical Hippo pathway, YAP is involved in cell proliferation and survival via transcriptional regulation related to SC proliferation, myelination, and remyelination during peripheral nerve development and regeneration [8,15,58]. Inactivation of YAP and the transcriptional coactivator with PDZ-binding motif (TAZ) in *Yap* ^{cHet};*Taz* ^{cKO} model mice did not affect myelin maintenance in adult SCs after nerve injury in a previous study [58]. These findings indicated that YAP was dispensable for myelin maintenance in adult nerves, although it is among the molecules essential for myelination during SC development. Moreover, blockade of the YAP upstream regulators MST1/2 by XMU successfully inhibited SC phenotype changes during WD and maintained the myelin structure, similar to that in intact nerves (Figs. 1 and 2). These findings suggested that 1) the canonical MST-LATS-YAP cascade is a subpathway of an important pathway in WD, or 2) WD involves multifactorial biochemical events (i.e., the Hippo pathway is not a unique WD-inhibiting pathway), demonstrating that XMU exerts effects on many potential drug targets (Fig. 6h).

First, we identified the MST1-RBP-miRNA pathway in SCs as an XMU-dependent noncanonical pathway. The crosstalk among noncanonical MST-RBP cascades in the Hippo pathway and miRNAs can affect SC myelination/differentiation during WD. Previously, Hippo signaling had

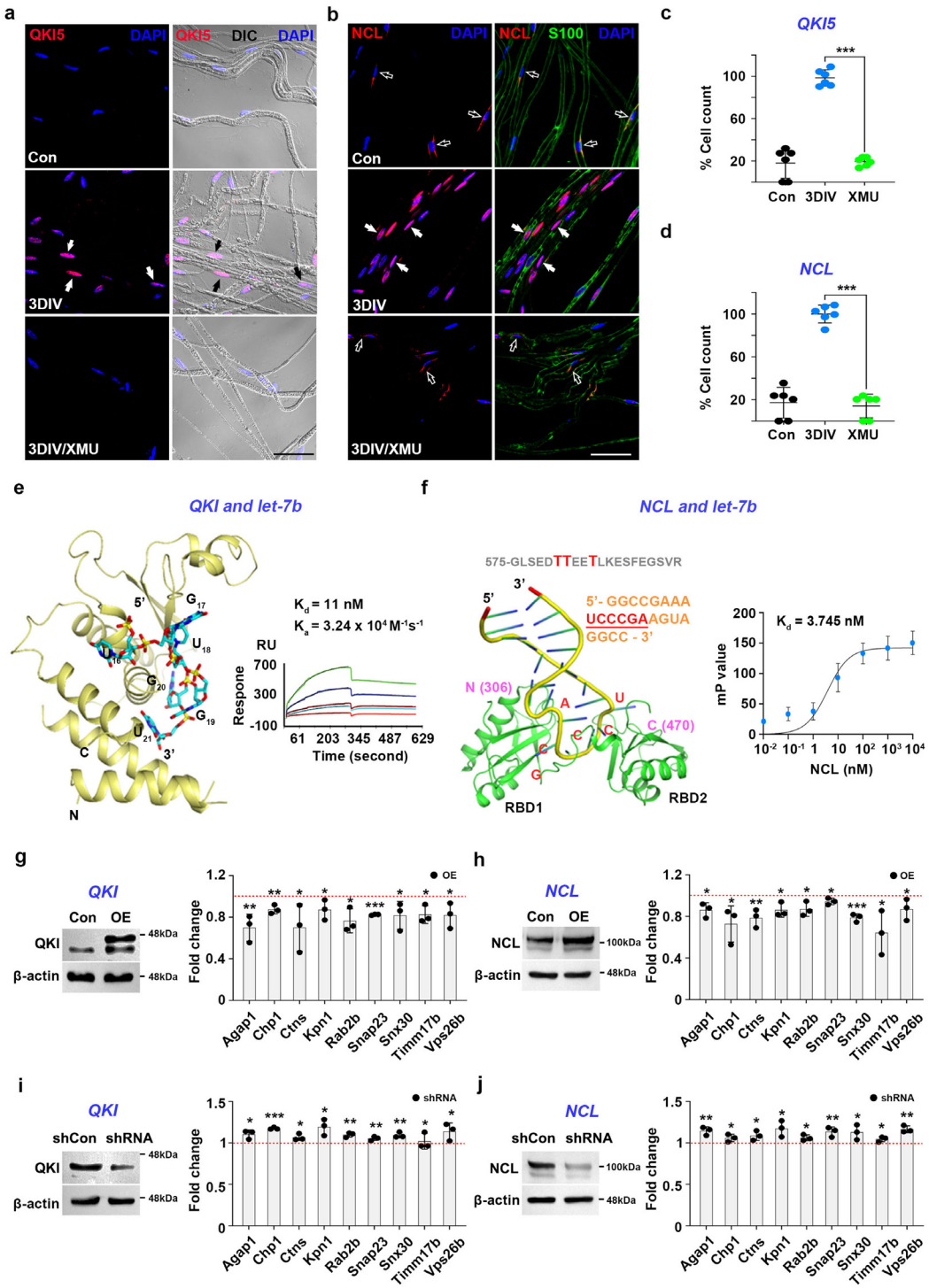

Fig. 5. MST1 phosphorylates QKI and NCL to modulate let-7b level in SCs. a Expression pattern of QKI5 in *ex vivo* nerve fibers with or without XMU treatment at 3DIV was assessed by immunostaining analysis. Arrows indicated QKI5/DAPI double-positive signals. Scale bar = 50 μm. **b** Immunostaining of NCL in *ex vivo* sciatic nerve fibers with or without XMU treatment at 3DIV. White arrows indicated the number of NCL/DAPI double-positive signals in each sample. Blank arrows showed NCL located around the nuclei, not in the nuclei. Scale bar = 50 μm. **c**, **d** Percentage of cell counts indicated the number of QKI5/DAPI (*c*) or NCL/DAPI (*d*) double-positive signals. **e** Molecular docking model of human QKI bound with a fragment of let-7b, UGUGGU (*left panel*). Surface Plasmon Resonance (SPR) profiles of recombinant human QKI proteins and let-7b with biotin label (*right panel*). **f** Crystal structure (*left panel*) of mouse NCL bound to NCL recognition element (NRE). The phosphorylated threonines are located outside of 306–470 a.a. range. Fluorescence polarization of let-7b-Cy3 bound to recombinant mouse NCL protein (*right panel*). Quaking, QKI; nucleolin, NCL. **g, h** At 48 h after transfection of empty vector or QKI/NCL plasmids, the lysates from SW10 cells were subjected to SDS-PAGE for Western blot analysis against QKI (*g*) or NCL (*h*) (*left panel*). Genes involving protein transport in total RNA from the transfected SW10 cells were detected by qRT-PCR (*right panel*). The 9 genes were downregulated after QKI/NCL overexpression. n = 3. **i, j** At 48 h after transfection of control and QKI/NCL shRNA in SW10, QKI (*i*) or NCL (*j*) from cell lysates were detected by Western blot (*left panel*). The genes involving protein transport were detected by qRT-PCR (*right panel*). The 9 genes were upregulated after QKI/NCL knockdown. n = 3. *p < 0.05, **p < 0.01, and ***p < 0.001.

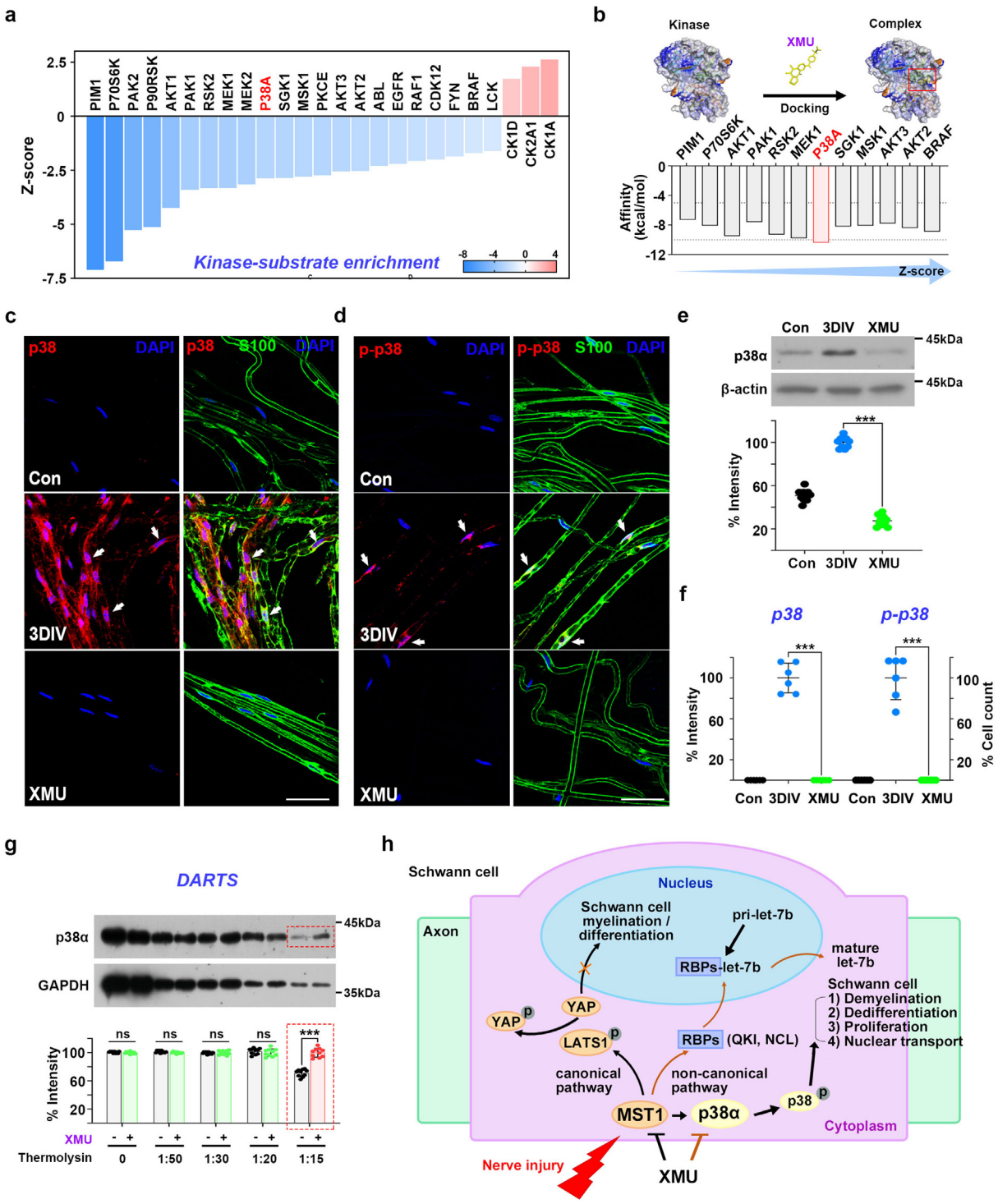

Fig. 6. XMU interacts with p38α protein kinase as its novel drug target in SCs. a Kinase-substrate enrichment analysis without phosphatases. Proteome normalized ratio of XMU/DMSO was taken to infer Z-score (kinase activation score). Red or blue presented kinases significantly activated and attenuated, respectively. **b** Binding affinity of XMU with the highly ranked 12 protein kinase targets. Affinity was defined as kcal/mol. p38α showed the strongest binding with XMU among the 12 kinases in **a**. **c, d** Expression patterns of p38α (*c*) and p-p38α (*d*) in *ex vivo* nerve fibers with or without XMU treatment at 3DIV were assessed by immunostaining analysis. Arrows indicated p38α or p-p38α/DAPI double-positive signals. Scale bar = 50 μm. **e** Western blot analysis of p38α was performed by using sciatic nerve explants. Graphs showed the intensities of immunoblots in each sample. **f** The left graph showed the intensities of p38α staining in sciatic nerve fibers cultured with 100 μM of XMU for 3DIV in **c**. Percentage of cell counts (*right panel*) indicated the number of p-p38α/DAPI-positive signals in **d**. **g** DARTS assay for target validation. Thermolysin-dependent p38α protein destabilization was suppressed by treatment and binding of XMU in SW10 cells. The graph (*lower panel*) is the quantification data shown in the Western blot (*upper panel*). **h** Schematic diagram of the polypharmacological mechanism of XMU. Back and brown arrows implied XMU-dependent canonical and non-canonical pathways, respectively, in SCs during WD. ***$p < 0.001$.

been discovered to affect widespread miRNA biogenesis, playing critical functions in SCs during WD [59,60].

In this study, we profiled XMU-dependent miRNAs in SCs and found that the mature miRNA let-7b regulated the abundance of mRNAs encoding protein transport molecules (Fig. 4 and Supplementary Fig. 4). Since a subset of RBPs modulates the biogenesis of miRNAs and the direct phosphorylation of RBPs via their upstream protein kinases to affect miRNA processing [61], it was previously demonstrated that MST1-dependent phosphorylation of QKI is involved in demyelination in the brain [62], and herein, we reveal an interaction between QKI and let7-b (Fig. 5 and Supplementary Fig. 7). Additionally, MST1-NCL-let-7b may be a novel noncanonical MST-RBP cascade, as NCL [19] was directly phosphorylated by MST1, bound to let-7b, overexpressed in the nuclei of SCs during WD, and regulated genes involved in protein transport (Fig. 5 and Supplementary Fig. 7). These results suggest that the noncanonical Hippo pathway consists of MST-QKI/NCL-let-7b cascades involved in protein transport during WD (Fig. 6h).

Among the protein kinases for which kinase-substrate enrichment was high (Fig. 6a), p21 activated kinase 1/2 (PAK1/2), AKT1-3, MEK1/2, serum/glucocorticoid regulated kinase 1 (SGK1), p38α, and mitogen- and stress-activated protein kinase 1 (MSK1) are involved in SC dynamics. PAK1/2 regulates the migration and transformation of SCs [63], while SGK1 and AKT1-3 are associated with SC myelination [64]. MEK1/2 and MSK1 are upstream kinases that phosphorylate extracellular signal-regulated protein kinase 1/2 (ERK1/2) and p38 MAPK, respectively, in SCs [65]. In particular, p38α, a possible polypharmacological effector of XMU, may exert greater regulatory effects on SC myelination/differentiation than other protein kinases. We demonstrated that p38α interacts with XMU via a DARTS analysis (Fig. 6g) and exhibited that the lowest affinity of p38α for XMU was mediated via hydrogen bonding at a p38α binding site consisting of amino acid residues E71 and T106 (Supplementary Fig. 9). XMU also effectively regulated the expression of both p38α and p-p38α (the active form) in *ex vivo* SCs during WD (Fig. 6c–f). Thus, the p38α pathway may be a specific pharmacological target of XMU in SCs, in addition to MST-LATS-YAP or MST-RBP-miRNA cascades (Fig. 6h).

Additionally, the MST1 signaling is mediated through the canonical MAPK subpathways, including the c-JUN N-terminal kinase 1 (JNK1) and p38 pathways, as kinases downstream of MST1 regulate cell death and apoptosis [66–68]. Since p38α is a well-characterized kinase regulating SC phenotype acquisition [23,69], XMU-dependent crosstalk of p38 with MST1/2 [70] may be indicate another noncanonical component of the Hippo pathway (Fig. 6). The nuclear translocation rate and total levels of c-JUN were clearly decreased in SCs after XMU treatment (Fig. 2b, e). Although c-JUN transcriptionally regulates YAP [71,72], YAP modulation of c-JUN translocation or expression has not been reported to date. Notably, in previous studies, XMU did not affect the phosphorylation of JNK [13], and p38α affected the phosphorylation of c-JUN [73]. These observations suggest that MST1 might be critical for noncanonical MST-p38 MAPK-c-JUN cascade activation in SCs or that the activation of c-JUN might be regulated by only p38MAPK in an MST-independent manner. All of these findings support the discovery of MST-independent signaling cascades regulated by XMU in SCs.

In our profiles of proteins, phosphopeptides, and miRNAs in SCs (Supplementary Tables 2, 4, 5), the term protein transport, nucleocytoplasmic transport, nuclear pore complex assembly, or protein import into the nucleus was commonly highly ranked in GO and KEGG enrichment analyses (Fig. 3 and Supplementary Figs. 3 and 8). Significantly, protein transport was enriched with upregulated proteins but not in the downregulated proteins (Fig. 3a). These results indicate that genes in intact or XMU-treated SCs relevant to nuclear import through which differentiated/myelinated conditions are maintained, may be upregulated, and gene expression may be posttranscriptionally regulated via miRNAs. YAP is translocated to the nuclei of SCs is regulated by the canonical Hippo pathway, which regulates transport across nuclear pores and maintains their myelinated/differentiated state [74,75]. Among proteins that are phosphorylated in an XMU-dependent manner and involved in nucleus–cytoplasm transport (Supplementary Fig. 8a, b), AHCTF1, RNABP2, and NUP98, as elements of the nuclear pore complex, are relevant to YAP nuclear transport, and AHCTF1 and RNABP2 were shown to be targeted by let-7 family miRNAs (Supplementary Table 5). These findings suggest that the nuclear translocation of YAP in SCs may be affected by post-transcriptional regulation of mRNAs encoding nuclear pore molecules in a noncanonical MST-RBP-let-7b-dependent manner as well as by regulation of YAP phosphorylation in a canonical MST-LATS-dependent manner.

Additionally, p38α phosphorylates nuclear pore proteins or karyopherins affecting nuclear transport [76,77], and we found that NUP153 and NUP214, known phosphorylation targets [78], were regulated in SCs in an XMU-dependent manner (Supplementary Table 5). Thus, the synergistic inhibition of Hippo/MST1 and p38α by XMU enhanced the nuclear transport of positive regulators such as YAP, which is involved in myelination [33] more efficiently than only MST1/2 inhibition in SCs during WD.

Overall, XMU is a potent inhibitor of MST1/2 and potentially targets p38α to regulate gene expression at multiple levels. In SCs, the affected cellular processes include cell differentiation, cell division cycle, cell proliferation, and fatty acid metabolism, which are related to common WD phenotypes (Fig. 3 and Supplementary Figs. 2, 3, 8). Aging, nuclear transport, the Hippo pathway, and MAPK signaling are also specifically regulated by XMU during WD (Fig. 3 and Supplementary Figs. 2, 3, 8). Transcriptomic and posttranscriptional changes govern Hippo/MST-dependent responses via direct phosphorylation of multiple RBPs in SCs. Thus, additional targeting of downstream components in the Hippo/MST pathway by XMU and promotion of its polypharmacological effects, including p38α-dependent responses, may improve the opportunity to develop noveltherapeutics for PNs in elderly individuals.

Ethics approval

All animal experiment procedures, including sacrifices, were approved by Kyung Hee University Committee of Animal Research [KHSASP-21-463] and progressed according to the guidance prepared by Korean Academy of Medical Science.

Available of data and materials

All datasets presented in this manuscript are available upon reasonable request from the corresponding author.

Funding

This work was supported by DGIST R&D program [24-CoE-BT-01] (to M-.S.K.), Medical University of South Carolina/University of Oklahoma startup fund and R01AA027532 (to J-.H.Y.), and Basic Science Research Program through the National Research Foundation of Korea (NRF) funded by the Ministry of Science, ICT and Future Planning [No. RS-2024-00333346/2020M3A9G710393422 (to J-.J.S.), No. 2022R1A2C2013377 (to M-.S.K.), No. 2022M3E5F2018597 (to B.P.), 2022R1A2C4001528 (to K-.W.M. and J.W.L), No. 2022R1F1A1073775 (to J.H.C.), No. 2021R1A2C1004184 (to H-.J.C) No. 2021R1A2C1004133 (to N.Y.J.) and No. 2023R1A2C1003763 (to J.J.)].

Author contributions

Hyung-Joo Chung: Conceived and designed the analysis, Collected the data, Wrote the paper. **Thy N.C. Nguyen:** Conceived and designed the analysis, Collected the data. **Ji Won Lee:** Conceived and designed the analysis, Collected the data. **Youngbuhm Huh:** Contributed data or analysis tools. **Seungbeom Ko:** Performed the analysis. **Heejin Lim:** Contributed data or analysis tools. **Hyewon Seo:** Contributed data or analysis tools. **Young-Geun Ha:** Contributed data or analysis tools.

Jeong Ho Chang: Performed the analysis. **Jae-Sung Woo:** Performed the analysis. **Ji-Joon Song:** Performed the analysis. **So-Woon Kim:** Performed the analysis. **Jin San Lee:** Performed the analysis. **Jung-Soon Mo:** Performed the analysis. **Boyoun Park:** Performed the analysis. **Kyung-Won Min:** Performed the analysis. **Je-Hyun Yoon:** Contributed data or analysis tools, Performed the analysis, Wrote the paper. **Min-Sik Kim:** Contributed data or analysis tools, Performed the analysis, Wrote the paper. **Junyang Jung:** Conceived and designed the analysis, Contributed data or analysis tools, Performed the analysis, Wrote the paper. **Na Young Jeong:** Conceived and designed the analysis, Contributed data or analysis tools, Performed the analysis, Wrote the paper.

Declaration of competing interest

The authors declare that they have no known competing financial interests or personal relationships that could have appeared to influence the work reported in this paper.

Acknowledgments

The authors thank Dr. Yoo Lim Chun, Dr. Waleed Twal, and Mr. Won-Joon Eom for technical assistance.

Appendix A. Supplementary data

Supplementary data to this article can be found online at https://doi.org/10.1016/j.neurot.2024.e00458.

References

[1] Waller A. Experiments on the section of the glosso-pharyngeal and hypoglossal nerves of the frog, and observations of the alterations produced thereby in the structure of their primitive fibres. Edinb Med Surg J 1851;76:369–76.
[2] Stoll G, Jander S, Myers RR. Degeneration and regeneration of the peripheral nervous system: from Augustus Waller's observations to neuroinflammation. J Peripher Nerv Syst 2002;7:13–27.
[3] Suzuki M. Peripheral neuropathy in the elderly. Handb Clin Neurol 2013;115:803–13.
[4] Brisset M, Nicola G. Peripheral neuropathies and aging. Geriatr Psychol Neuropsychiatr Vieil 2018;16:409–13.
[5] Tricaud N, Park HT. Wallerian demyelination: chronicle of a cellular cataclysm. Cell Mol Life Sci 2017;74:4049–57.
[6] Tauseef M, Aqil M. Molecular mechanisms regulating wallerian degeneration. In: Radosevich JA, editor. Apoptosis and beyond: the many ways cells die. 1st edn 2018. p. 205–24. Ch.11.
[7] Grigoryan T, Stein S, Qi J, Wende H, Garratt AN, Nave KA, et al. Wnt/Rspondin/β-catenin signals control axonal sorting and lineage progression in Schwann cell development. Proc Natl Acad Sci USA 2013;110:18174–9.
[8] Harvey KF, Zhang X, Thomas DM. The Hippo pathway and human cancer. Nat Rev Cancer 2013;13:246–57.
[9] Ma S, Meng Z, Chen R. The Hippo pathway: biology and pathophysiology. Annu Rev Biochem 2019;88:577–604.
[10] Nishio M, Miyachi Y, Otani J, Tane S, Omori H, Ueda F, et al. Hippo pathway controls cell adhesion and context dependent cell competition to influence skin engraftment efficiency. Faseb J 2019;33:5548–60.
[11] Ogata T, Iijima S, Hoshikawa S, Miura T, Yamamoto SI, Oda H, et al. Opposing extracellular signal-regulated kinase and Akt pathways control schwann cell myelination. J Neurosci 2004;24:6724–32.
[12] Herculano-Houzel S. The glia/neuron ratio: how it varies uniformly across brain structures and species and what that means for brain physiology and evolution. Glia 2014;62:1377–91.
[13] Fan F, He Z, Kong L-L, Chen Q, Yuan Q, Zhang S, et al. Pharmacological targeting of kinases MST1 and MST2 augments tissue repair and regeneration. Sci Transl Med 2016;8:352ra108.
[14] Triastuti E, Nugroho AB, Zi M, Prehar S, Kohar YS, Bui TA, et al. Pharmacological inhibition of Hippo pathway, with the novel kinase inhibitor XMU-MP-1, protects the heart against adverse effects during pressure overload. Br J Pharmacol 2019;176:3956–71.
[15] Poitelon Y, Lopez-Anido C, Catignas K, Berti C, Palmisano M, Williamson C, et al. YAP and TAZ control peripheral myelination and the expression of laminin receptors in Schwann cells. Nat Neurosci 2016;19:879–87.
[16] Zealy RW, Wrenn SP, Davila S, Min K, Yoon J. microRNA-binding proteins: specificity and function. Wiley interdiscip Rev RNA 2017;8:1–8.
[17] Park BS, Kim HW, Rhyu IJ, Park C, Yeo SG, Huh Y, et al. Hydrogen sulfide is essential for Schwann cell responses to peripheral nerve injury. J Neurochem 2015;132:230–42.
[18] Chun YL, Park KH, Pallavi B, Eom WJ, Park C, Huh Y, et al. Novel cinnamaldehyde derivatives inhibit peripheral nerve degeneration by targeting schwann cells. Antioxidants 2022;11:1846.
[19] Lee TA, Han H, Polash A, Cho SK, Lee JW, Ra EA, et al. The nucleolus is the site for inflammatory RNA decay during infection. Nat Commun 2022;13:5203.
[20] Cruz-Gallardo I, Aroca Á, Gunzburg MJ, Sivakumaran A, Yoon JH, Angulo J, et al. The binding of TIA-1 to RNA C-rich sequences is driven by its C-terminal RRM domain. RNA Biol 2014;11:766–76.
[21] Grove M, Lee H, Zhao H, Son YJ. Axon-dependent expression of yap/taz mediates schwann cell remyelination but not proliferation after nerve injury. Elife 2020;9:e50138.
[22] Parkinson DB, Bhaskaran A, Arthur-farraj P, Noon LA, Woodhoo A, Lloyd AC, et al. c-Jun is a negative regulator of myelination. J Cell Biol 2008;181:625–37.
[23] Yang DP, Kim J, Syed N, Tung Y, Bhaskaran A, Mindos T, et al. p38 MAPK activation promotes denervated schwann cell phenotype and functions as a negative regulator of schwann cell differentiation and myelination. J Neurosci 2012;32:7158–68.
[24] D'Antonio M, Droggiti A, Feltri ML, Roes J, Wrabetz L, Mirsky R, et al. TGFβ type II receptor signaling controls schwann cell death and proliferation in developing nerves. J Neurosci 2006;26:8417–27.
[25] Duan Y, He X, Yang H, Ji Y, Tao T, Chen J, et al. D3/CDK11p58 complex involved in schwann cells proliferation repression caused by lipopolysaccharide. Inflammation 2010;33:189–99.
[26] Hertz L, Chen Y, Waagepetersen HS. Effects of ketone bodies in Alzheimer's disease in relation to neural hypometabolism, β-amyloid toxicity, and astrocyte function. J Neurochem 2015;134:7–20.
[27] Kim HA, Ratner N, Roberts TM, Stiles CD. Schwann cell proliferative responses to cAMP and Nf1 are mediated by cyclin D1. J Neurosci 2001;21:1110–6.
[28] Liu JH, Tang Q, Li X-X, Qi J, Zeng R-X, Zhu Z-W, et al. Analysis of transcriptome sequencing of sciatic nerves in Sprague-Dawley rats of different ages. Neural. Regen. Res 2018;13:2182–90.
[29] Lu PJ, Wang G, Cai XD, Zhang P, Wang HK. Sequencing analysis of matrix metalloproteinase 7-induced genetic changes in Schwann cells. Neural. Regen. Res. 2020;15:2116–22.
[30] Tsujii M, Akeda K, Iino T, Uchida A. Are BMPs involved in normal nerve and following transection?: a pilot study. Clin Orthop Relat Res 2009;467:3183–9.
[31] van Vliet AC, Lee J, van der Poel M, Mason MRJ, Noordermeer JN, Fradkin LG, et al. Coordinated changes in the expression of Wnt pathway genes following human and rat peripheral nerve injury. PLoS One 2021;16:e0249748.
[32] Wang Y, Tang X, Yu B, Gu Y, Yuan Y, Yao D, et al. Network revealed involvements of Birc2, Birc3 and Tnfrsf1a in anti-apoptosis of injured peripheral nerves. PLoS One 2012;7:e43436.
[33] Jessen KR, Mirsky R. Negative regulation of myelination: relevance for development, injury, and demyelinating disease. Glia 2008;56:1552–65.
[34] Li M, Banton MC, Min Q, Parkinson DB, Dun X. Meta-analysis reveals transcription factor upregulation in cells of injured mouse sciatic nerve. Front Cell Neurosci 2021;15:688243.
[35] Van Dam H, Castellazzi M. Distinct roles of Jun: Fos and Jun: ATF dimers in oncogenesis. Oncogene 2001;20:2453–64.
[36] Piñero J, Bravo À, Queralt-Rosinach N, Gutiérrez-Sacristán A, Deu-Pons J, Centeno E, et al. DisGeNET: a comprehensive platform integrating information on human disease-associated genes and variants. Nucleic Acids Res 2017;45:D833–9.
[37] He Y, Kim JY, Dupree J, Tewari A, Melendez-Vasquez C, John S, et al. Yy1 as a molecular link between neuregulin and transcriptional modulation of peripheral myelination. Nat Neurosci 2010;13:1472–80.
[38] Bartel DP. MicroRNAs: genomics, biogenesis, mechanism, and function. Cell 2024;116:281–97.
[39] Bartel DP. Metazoan MicroRNAs. Cell 2019;173:20–51.
[40] Elkayam E, Kuhn CD, Tocilj A, Haase AD, Greene EM, Hannon GJ, et al. The structure of human argonaute-2 in complex with miR-20a. Cell 2012;150:100–10.
[41] Kwon SC, Nguyen TA, Choi YG, Jo MH, Hohng S, Kim VN, et al. Structure of human DROSHA. Cell 2016;164:81–90.
[42] Liu Z, Wang J, Cheng H, Ke X, Sun L, Zhang QC, et al. Cryo-EM structure of human dicer and its complexes with a pre-miRNA substrate. Cell 2018;173:1191–203.
[43] Partin AC, Zhang K, Jeong BC, Herrell E, Li S, Chiu W, et al. Cryo-EM structures of human Drosha and DGCR8 in complex with primary MicroRNA. Mol Cell 2020;78:411–22.
[44] Hu X, Li Y, Zhang T, Li L, Chen S, Wu X, et al. Phosphorylation of Ago2 is required for its role in DNA double-strand break repair. J. Genet. Genomics 2021;48:333–40.
[45] Zhou X, He C, Ren J, Dai C, Stevens SR, Wang Q, et al. Mature myelin maintenance requires Qki to coactivate PPARβ-RXRα-mediated lipid metabolism. J Clin Invest 2020;130:2220–36.
[46] Ginisty H, Sicard H, Roger B, Bouvet P. Structure and functions of nucleolin. J Cell Sci 1999;112:761–72.
[47] Jerke U, Tkachuk S, Kiyan J, Stepanova V, Kusch A, Hinz M, et al. Stat1 nuclear translocation by Nucleolin upon Monocyte differentiation. PLoS One 2009;4:e8302.
[48] Abdelmohsen K, Gorospe M. RNA-binding protein nucleolin in disease. RNA Biol 2012;9:799–808.
[49] Ciafrè SA, Galardi S. microRNAs and RNA-binding proteins: a complex network of interactions and reciprocal regulations in cancer. RNA Biol 2013;10:934–42.
[50] Pickering BF, Yu D, Van Dyke MW. Nucleolin protein interacts with microprocessor complex to affect biogenesis of microRNAs 15a and 16. J Biol Chem 2011;286:44095–103.
[51] Wang Y, Vogel G, Yu Z, Richard S. The QKI-5 and QKI-6 RNA binding proteins regulate the expression of MicroRNA 7 in glial cells. Mol Cell Biol 2013;33:1233–43.

[52] Huang F, Wu Y, Tan H, Guo T, Zhang K, Li D, et al. Phosphorylation of nucleolin is indispensable to its involvement in the proliferation and migration of non-small cell lung cancer cells. Oncol Rep 2019;41:590–8.
[53] Lamprou M, Koutsioumpa M, Kaspiris A, Zompra K, Tselios T, Papadimitriou E. Binding of pleiotrophin to cell surface nucleolin mediates prostate cancer cell adhesion to osteoblasts. Tissue Cell 2022;76:101801.
[54] Sletten T, Kostas M, Bober J, Sorensen V, Yadollahi M, Olsnes S, et al. Nucleolin regulates phosphorylation and nuclear export of Fibroblast Growth Factor 1 (FGF1). PLoS One 2014;9:e90687.
[55] Arter J, Wegner M. Transcription factors Sox10 and Sox2 functionally interact with positive transcription elongation factor b in Schwann cells. J Neurochem 2015;132:384–93.
[56] Harty BL, Coelho F, Pease-Raissi SE, Mogha A, Ackerman SD, Herbert AL, et al. Myelinating Schwann cells ensheath multiple axons in the absence of E3 ligase component Fbxw7. Nat Commun 2019;10:2976.
[57] Lomenick B, Hao R, Jonai N, Chin RM, Aghajan M, Warburton S, et al. Target identification using drug affinity responsive target stability (DARTS). Curr. Protoc. Chem. Biol. 2011;3:163–80.
[58] Jeanette H, Marziali LN, Bhatia U, Hellman A, Herron J, Kopec AM, et al. YAP andTAZ regulate Schwann cell proliferation and differentiation during peripheral nerve regeneration. Glia 2021;69:1061–74.
[59] Mori M, Triboulet R, Mohseni M, Schlegelmilch K, Shrestha K, Camargo FD, et al. Signaling regulates microprocessor and links cell-density-dependent miRNA biogenesis to cancer. Cell 2014;156:893–906.
[60] Viader A, Chang LW, Fahrner T, Nagarajan R, Milbrandt J. MicroRNAs modulate Schwann cell response to nerve injury by reinforcing transcriptional silencing of dedifferentiation-related genes. J Neurosci 2011;31:17358–69.
[61] Shukla GC, Singh J, Barik S. MicroRNAs: processing, maturation, target recognition and regulatory functions. Mol Cell Pharmacol 2011;3:83–92.
[62] Ren J, Dai C, Zhou X, Barnes JA, Chen X, Wang Y, et al. Qki is an essential regulator of microglial phagocytosis in demyelination. J Exp Med 2021;218:e20190348.
[63] Flaiz C, Chernoff J, Ammoun S, Peterson JR, Hanemann CO. PAK kinase regulates Rac GTPase and is a potential target in human schwannomas. Exp Neurol 2009;218:137–44.
[64] Okura A, Inoue K, Sakuma E, Takase H, Ueki T. SGK1 in Schwann cells is a potential molecular switch involved in axonal and glial regeneration during peripheral nerve injury. Biochem Biophys Res Commun 2022;607:158–65.
[65] Ammoun S, Ristic N, Matthies C, Hilton DA, Hanemann CO. Targeting ERK12 activation and proliferation in human primary schwannoma cells with MEK12 inhibitor AZD6244. Neurobiol Dis 2010;37:141–6.
[66] Lee JK, Shin JH, Hwang SG, Gwag BJ, McKee AC, Lee J, et al. MST1 functions as a key modulator of neurodegeneration in a mouse model of ALS. Proc Natl Acad Sci USA 2013;110:12066–71.
[67] Qiao M, Wang Y, Xu X, Lu J, Dong Y, Tao W, et al. Mst1 is an interacting protein that mediates PHLPPs' induced apoptosis. Mol Cell 2010;38:512–23.
[68] Ura S, Masuyama N, Graves JD, Gotoh Y. MST1-JNK promotes apoptosis via caspase-dependent and independent pathways. Gene Cell 2001;6:519–30.
[69] Sheridan L, Dun X, Dee G, Gray B, Mindos T, Parkinson DB. The role of p38alpha in Schwann cells in regulating peripheral nerve myelination and repair. J Neurochem 2017;141:37–47.
[70] Richters A, Doyle SK, Freeman DB, Lee C, Leifer BS, Jagannathan S, et al. Modulating androgen receptor-driven transcription in prostate cancer with selective CDK9 inhibitors. Cell Chem Biol 2021;28:134–47.
[71] Qiao Y, Qian Y, Wang J, Tang X. Melanoma cell adhesion molecule stimulates yes-associated protein transcription by enhancing CREB activity via c-Jun/c-Fos in hepatocellular carcinoma cells. Oncol Lett 2016;11:3702–8.
[72] Zhang J, Wong CC, Leung KT, Wu F, Zhou Y, Tong JHM, et al. FGF18–FGFR2 signaling triggers the activation of c-Jun–YAP1 axis to promote carcinogenesis in a subgroup of gastric cancer patients and indicates translational potential. Oncogene 2020;39:6647–63.
[73] Humar M, Loop T, Schmidt R, Hoetzel A, Roesslein M, Andriopoulos N, et al. The mitogen-activated protein kinase p38 regulates activator protein 1 by direct phosphorylation of c-Jun. Int J Biochem Cell Biol 2007;39:2278–88.
[74] Elosegui-Artola A, Andreu I, Beedle AEM, Lezamiz A, Uroz M, Kosmalska AJ, et al. Force triggers YAP nuclear entry by regulating transport across nuclear pores. Cell 2017;171:1397–410.
[75] Rapoport TA, Jungnickel B, Kutay U. Protein transport across the eukaryotic endoplasmic reticulum and bacterial inner membranes. Annu Rev Biochem 1996;65:271–303.
[76] Dashti S, Taherian-Esfahani Z, Kholghi-Oskooei V, Noroozi R, Arsang-Jang S, Ghafouri-Fard S, et al. In silico identification of MAPK14-related lncRNAs and assessment of their expression in breast cancer samples. Sci Rep 2020;10:8316.
[77] Liu J, Yu X, Liu B, Yu H, Li Z. Phosphorylated mapk14 promotes the proliferation and migration of bladder cancer cells by maintaining runx2 protein abundance. Cancer Manag Res 2020;12:11371–82.
[78] Porter FW, Brown B, Palmenberg AC. Nucleoporin phosphorylation triggered by the encephalomyocarditis virus leader protein is mediated by mitogen-activated protein kinases. J Virol 2010;84:12538–48.